Biosensors and Bioelectronics 127 (2019) 38–44

Contents lists available at ScienceDirect

Biosensors and Bioelectronics

journal homepage: www.elsevier.com/locate/bios

Photoelectrochemical biosensor for hydroxymethylated DNA detection and T4-β-glucosyltransferase activity assay based on WS_2 nanosheets and carbon dots

Chengji Sui[a,1], Tingting Wang[b,1], Yunlei Zhou[a,*], Huanshun Yin[a,*], Xiangjian Meng[a], Shenran Zhang[a], Geoffrey I.N. Waterhouse[a,e], Qin Xu[c,d,**], Yuping Zhuge[b], Shiyun Ai[a]

[a] College of Chemistry and Material Science, Shandong Agricultural University, Taian 271018, PR China
[b] College of Resources and Environment, Shandong Agricultural University, Taian 271018, PR China
[c] School of Chemistry and Chemical Engineering, Yangzhou University, Yangzhou 225002, PR China
[d] Guangling College, Yangzhou University, Yangzhou 225002, PR China
[e] School of Chemical Sciences, The University of Auckland, Auckland 1142, New Zealand

ARTICLE INFO

Keywords:
Photoelectrochemical biosensor
DNA hydroxymethylation
β-Glucosyltransferase
WS_2 nanosheets
Carbon dots

ABSTRACT

5-Hydroxymethylcytosine (5hmC) plays an important role in switching genes on and off in mammals, and it is implicated in both embryonic development and cancer progression. Herein, a novel photoelectrochemical (PEC) biosensor was developed for 5hmC detection based on WS_2 nanosheets as the photoactive material and boronic acid functionalized carbon dots (B-CDs) for signal amplification unit. This biosensor can also be used for T4-β-glucosyltransferase (β-GT) activity assessment. Firstly, WS_2 nanosheets and gold nanoparticles (AuNPs) were immobilized on an ITO electrode surface. Then probe DNA was immobilized on this electrode surface via Au-S bond. Afterwards, the complementary DNA containing 5hmC was then captured on the modified electrode surface by hybridization. Subsequently, β-GT transferred glucose from uridine diphosphoglucose to the hydroxyl groups of the 5hmC residues. After glycosylation, B-CDs could further be immobilized on the modified electrode surface resulting in a strong photocurrent. The PEC biosensor afforded high selectivity, excellent sensitivity and good reproducibility, with detection limits of 0.0034 nM and 0.028 unit/mL for 5hmC and β-GT, respectively. Results demonstrate that the photoelectrochemical strategy introduced here based on WS_2 nanosheets and B-CDs offers a versatile platform for hydroxymethylated DNA detection, β-GT activity assessment and β-GT inhibitor screening.

1. Introduction

5-Hydroxymethylcytosine (5hmC) is now considered to be the sixth base of DNA (Münzel et al., 2011), and it is formed from 5-methylcytosine (5mC) via the catalytic action of ten-eleven translocation (TET) proteins. Studies have shown that 5hmC is found in relatively high levels in neuron cells and embryonic stem cells, suggesting that it plays important roles in embryonic development, nuclear reprogramming, regulating gene expression and cancer progression in mammals (Kriaucionis and Heintz, 2009). Since 5hmC is typically found in very low level in cells, very sensitive methods are required for its detection.

Many analytical methods have been developed for 5hmC detection and quantification, including fluorescence (Chen et al., 2017), high performance liquid chromatography-mass spectrometry (HPLC-MS/MS) (Yin et al., 2015), single-molecule real-time (SMRT) sequencing (Flusberg et al., 2010), and thin layer chromatography (TLC) (Ito et al., 2010). However, all these methods have one or more of the following limitations: low sensitivity, poor selectivity, complicated sample preparation protocol or high equipment cost. Therefore, simple, low-cost, fast and ultrasensitive methods for detection of 5hmC are demanded.

The detection of 5hmC is challenging due to its structural similarity with 5mC. However, T4-β-Glucosyltransferase (β-GT) can specifically recognize 5hmC by transferring a glucose molecule from a glucose donor (uridine diphosphoglucose, UDP-Glu) to the hydroxyl group of 5hmC (Sukovich et al., 2015). After glycosylation, the glucose molecule can be used as linker to introduce additional functional group, such as a

* Corresponding authors.
** Corresponding author at: School of Chemistry and Chemical Engineering, Yangzhou University, Yangzhou 225002, PR China.
E-mail addresses: zhyl@sdau.edu.cn (Y. Zhou), yinhs@sdau.edu.cn (H. Yin), xuqin@yzu.edu.cn (Q. Xu).
[1] These authors contributed equally to this work.

https://doi.org/10.1016/j.bios.2018.11.054
Received 17 October 2018; Received in revised form 26 November 2018; Accepted 28 November 2018
Available online 07 December 2018
0956-5663/

fluorescent tag or signaling molecule. For example, Chen et al. used β-GT to transfer glucose onto 5hmC, which was immobilized on an electrode surface. The glucose molecule could then be oxidized by sodium periodate to produce an aldehyde, which could then react with the biotin modified aldehyde reaction probe. Through the reaction between biotin and streptavidin, horseradish peroxidase (linked to the streptavidin) could further be captured on the electrode surface, thereby allowing sensitive detection of 5hmC (Chen et al., 2016). Sun et al. also presented a method based on specific transfer of a glucose moiety to the hydroxyl group of 5hmC by β-GT. The presence of glucose moiety can prevent DNA strand scission by *Msp*I restriction endonuclease, resulting in a decreased ECL signal that was used as the basis for the detection of 5hmC (Sun et al., 2016). Our group has also used β-GT as specific recognition agent in the fabrication of biosensors for 5hmC detection (Yin et al., 2017).

Photoelectrochemical (PEC) biosensors are becoming increasingly popular due to their low-cost, fast analysis and high sensitivity. Photoelectrochemistry not only has electrochemical advantages (Guo, 2016, 2017; Guo et al., 2018; Guo and Ma, 2017), but also possesses higher sensitivity and lower background signal compared with electrochemistry due to the total separation and the different energy forms of the excitation source and the detection signal. PEC methods rely on the separation and charges (electrons and holes) in semiconducting photoactive materials under light illumination (i.e. photon-to-electrical signal conversion) (Zhao et al., 2014). PEC analyses have been used in the biochemical field for the detection of microRNA (Hou et al., 2018), protein kinase A activity (Li et al., 2017a), oxytetracycline (Li et al., 2017b) and also acetylcholinesterase activity measurement (Hou et al., 2016). Thus, PEC technique might be a ideal platform for 5hmC detection.

Many different photovoltaic materials have been used in PEC biosensors, including g-C_3N_4, MoS_2, TiO_2, Bi_2S_3 and BiOI (Ge et al., 2016; Okoth et al., 2016; Yan et al., 2015; Zang et al., 2016). Recently, two-dimensional transition metal chalcogenides have attracted intense interest due to their unique chemical, physical and electronic properties (Mo et al., 2017). Among them, WS_2 displays excellent performance when it is incorporated into biosensing platform due to its good biocompatibility, high loading efficiency for biomolecules arising from its 2D nanosheet morphology, and its ease of processing (e.g. high dispersibility in aqueous solution). In addition, WS_2 can be easily exfoliated into ultrathin nanosheets owing to its layered structure which is characterized by strong in-plane W-S bonding and weak van der Waals interactions between planes (Tan et al., 2018). WS_2 nanosheets offer numerous advantages such as high specific surface area, good dispersibility in polar media, good conductivity, narrow band gap allowing good solar spectrum utilization, and excellent photoelectrochemical performance (Ge et al., 2017).

In this work, we aimed to exploit the excellent properties of WS_2 nanosheets in the development of a multi-functional PEC biosensor for the simultaneous detection of 5hmC and β-GT activity. WS_2 nanosheets were obtained by the sonication-assisted liquid exfoliation of WS_2 in water containing poly(acrylic acid) (PAA). Strong coordination between the carboxyl groups of PAA with tungsten atoms of layered WS_2 promotes nanosheet formation. A PEC biosensor was then constructed using WS_2 nanosheets as the photoactive component, which also employed β-GT as the specific recognition unit of 5hmC and boronic acid functionalized carbon dots (B-CDs) as signal amplification unit. Scheme 1 depicts the construction of the novel PEC biosensor for 5hmC detection and β-GT activity assay. WS_2 nanosheets were used as photoactive material and deposited on an ITO electrode surface, thereby providing a stable photocurrent response. Then, gold nanoparticles (AuNPs) were modified on the WS_2/ITO electrode by physical adsorption. The modified AuNPs can not only improve the photocurrent response, but also provide an attachment site for probe DNA immobilization via the formation of Au-S bonds between the AuNPs and –SH groups of probe DNA. After introducing the probe DNA, complementary DNA containing 5hmC was captured on the electrode surface via hybridization with probe DNA. Next, the electrode was incubated with β-GT, which transferred a glucose molecule from UDP-Glu to the hydroxyl group of the 5hmC residues. Subsequently, boronic acid can covalently bind with 1,2-diol groups of the carbohydrates (such as glucose) to form esters. Accordingly, boronic acid functionalized carbon dots (B-CDs) were employed here for signal amplification. The immobilization of B-CDs accelerated spatial charge separation in the biosensor, thereby increasing the photocurrent response. The strategy introduced here proved very effective for the detection of 5hmC and assay of β-GT activity, confirming the potential of PEC biosensors in these applications.

2. Experimental

2.1. Reagents and apparatus

Chloroauric acid tetrahydrate ($HAuCl_4{\cdot}4H_2O$), phenylboronic acid, PAA, sodium citrate, 4-phenylimidazole, NaH_2PO_4, Na_2HPO_4, $NH_3{\cdot}H_2O$, and NaOH were ordered from Aladdin (Shanghai, China). Tungsten disulfide (WS_2), 6-Mercapto-1-hexanol (MCH) and dithiothreitol (DTT) were sourced from Sigma-Aldrich (USA). T4-β-Glucosyltransferase (β-GT) and UDP-Glu were purchased from Takara Biotechnology Co., Ltd. (China). 4-galactosyltransferase 6 protein (β-GAT) and Recombinant Human UGT2B7 protein were offered by Abcam (Cambridge, UK). DNA sequences were provided by Sangon (Shanghai, China). Base sequences were as follows: 5'-CGC GCG TAC ATC GGC CAC ATC T-SH-3' (probe DNA); 5'-AGA TGT GGC CGA TGT ACG C^{hm}GC G-3' (complementary hydroxymethylated DNA, 5hmC-DNA); 5'-AGA TGT GGC CGA TGT ACG C^{m}GC G-3' (complementary methylated DNA, 5mC-DNA); 5'-AGA UGU GGC CGA UGU ACG C^{m}GC G-3' (complementary methylated RNA, 5mC-RNA). ITO conductive glass was supplied by Zhuhai Kaivo Electronic Components Co., Ltd. (Zhuhai, China, ITO coating 180 ± 25 nm, sheet resistance < 15 Ω/cm^2). Buffer solutions used were as follows: Probe DNA immobilization buffer, 10 mM Tris-HCl, 1.0 mM EDTA, 1.0 M NaCl, and 1.0 mM TCEP (pH = 7.0). DNA hybridization buffer, 10 mM Tris-HCl, 1.0 mM EDTA, and 1.0 M NaCl (pH = 7.4). β-GT storage buffer, 20 mM potassium phosphate (pH = 7.0) containing 0.2 M NaCl, 0.1 mM EDTA, 0.25 mM DTT, 50% glycerol. 1 × β-GT reaction buffer, 10 mM Tris-HCl, 50 mM NaCl, 10 mM $MgCl_2$, 1 mM DTT (pH = 7.9). Washing buffer, 10 mM Tris-HCl containing 50 mM NaCl (pH = 7.4). PEC detection buffer, 0.1 M PBS containing 0.1 M AA (pH = 7.4). EIS detection buffer, 10 mM PBS containing 5 mM $K_3[Fe(CN)_6]$, 5 mM $K_4[Fe(CN)_6]$ and 0.1 M KCl (pH = 7.4).

Transmission electron microscopy (TEM) images were obtained on a Tecnai G2 F20 instrument (USA). Scanning electron microscopy (SEM) images were collected on a Quanta Q400 (USA). PEC measurements were performed on a CHI832A electrochemical workstation (CH Instruments, Austin, USA). A three-electrode system was used in the PEC experiments, comprising a modified ITO electrode as the working electrode, a Pt wire as the counter electrode and a standard calomel electrode as the reference electrode. PEC experiments were carried out on a home-built PEC system, which was equipped with a 500 W Xe lamp as the irradiation source. PEC measurements were performed at a potential of −0.3 V in a detection buffer containing 0.1 M PBS and 0.1 M AA (pH = 7.4). Electrochemical impedance spectroscopy (EIS) measurements were carried out at a CHI660C electrochemical workstation (CH Instruments, Austin, USA).

2.2. Preparation of WS_2 nanosheets, AuNPs and B-CDs

See Supplementary Materials.

2.3. Biosensor fabrication

ITO conductive glass slides were cut into 1.0 × 5.0 cm^2 pieces and

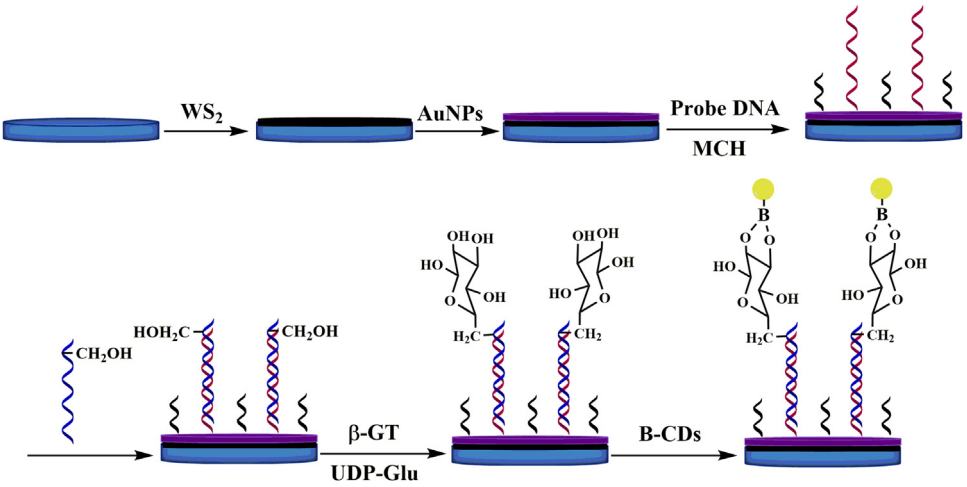

Scheme 1. Schematic diagram of the PEC biosensor construction process.

cleaned via sonication for 15 min in acetone, then NaOH solution (1 M, in 50 vol% ethanol), then distilled deionized water, followed by thorough washing with double distilled water. The effective area of the ITO electrode is 0.195 cm^2 and the electrode was contacted with electrochemical workstation using wire. The ITO pieces were then dried in air. Layered WS_2 nanosheets (3 mg) were ultrasonically dispersed in 1 mL of double distilled deionized water, after which 40 μL of the suspension was dropped onto a piece of ITO and dried under an infrared lamp. The resulting electrode is denoted as WS_2/ITO. Then, the electrode was rinsed with washing buffer for three times. After that, 40 μL of the AuNPs dispersion was placed on the electrode surface and dried under an infrared lamp (affording AuNPs/WS_2/ITO). Then, the electrode was rinsed with washing buffer for three times. For the probe DNA self-assembly, 40 μL of a 1 μM probe DNA solution in probe DNA immobilization buffer was dropped on electrode surface and incubated for 2 h in a humid chamber at 37 °C. The electrode was then rinsed three times with washing buffer to remove any unreacted probe DNA (yielding ssDNA/AuNPs/WS_2/ITO). Afterwards, 40 μL of 0.1 mM MCH solution was dropped on the electrode surface and the electrode incubated for 0.5 h. The obtained electrode was rinsed three times with washing buffer. The probe DNA was then hybridized with 20 μL of complementary target DNA with the 5hmC modification (varying concentrations) in DNA hybridization buffer for 2 h at 37 °C. The obtained 5hmC-dsDNA/AuNPs/WS_2/ITO electrode was then rinsed three times with washing buffer. Next, 20 μL of 1X T4 β-glucosyltransferase reaction buffer containing 40 mM UDP-glucose and 60 unit/mL β-GT was dropped onto the electrode surface and the electrode incubated for 2 h at 37 °C. The obtained electrode (Glu/5hmC-dsDNA/AuNPs/WS_2/ITO) was rinsed with washing buffer three times. Finally, the electrode was incubated with 40 μL of the B-CDs dispersion for 1 h at room temperature, then washed three times with washing buffer. The final modified electrode is denoted as B-CDs/Glu/5hmC-dsDNA/AuNPs/WS_2/ITO.

3. Results and discussion

3.1. Characterization of materials

The WS_2 nanosheets were characterized by TEM, AFM and Raman spectroscopy. TEM and AFM analyses reveal that the WS_2 nanosheets have layered structure (Fig. 1A, Fig. 1F), with the thickness of layers being around 2 nm (around three WS_2 nanosheet layers) (Xu et al., 2015). Some single layer sheets were also produced during the exfoliation process. Two Raman bands at 351 and 422 cm^{-1} are observed for the WS_2 nanosheets (Fig. 1D), corresponding to in plane (E_{2g} mode) and out of plane (A_{1g}) vibrations of WS_2, respectively. The B-CDs possess spherical morphology (Fig. 1B), with the HRTEM image (inset) showing lattice spacings of 0.33 nm, which could readily be indexed to graphene (002) planes. The FT-IR spectrum of the B-CDs (Fig. 1E) contains peaks at 3500, 3125, 1340–1400, 1168 and 1084 cm^{-1}, which are assigned to O-H stretching (C-OH or H_2O), O-H stretching (B-O-H), B-O stretching, B-O-H bending and C-B stretching vibrations, respectively (Xie et al., 2018). These observations of all these IR-active vibrations confirm that the surfaces of the CDs are heavily functionalized with boronic acid groups. The AuNPs prepared by the citrate reduction method display a characteristic spherical morphology with an average diameter around 10 nm (Fig. 1C).

3.2. Characterization of the modified electrodes

EIS was used to follow the stepwise fabrication of the PEC biosensor (Fig. 2A). The bare ITO electrode shows an interface electron transfer impedance (R_{et}) of about 240 Ω (curve a). After the WS_2 was coated on the ITO electrode, a larger semi-circle with a R_{et} of about 600 Ω was obtained (curve b). The increase in the R_{et} is attributed to negative charge on the surface of WS_2 nanosheets, which hinders the diffusion of the redox probe to the electrode. After deposition of the AuNPs (curve c), the R_{et} value decreases slightly which can be explained by the excellent electrical conductivity of gold. When the probe DNA was captured on the electrode surface, the R_{et} value increases considerably (curve d). This is expected, since the immobilized probe DNA possesses a large volume and is insulating, both of which would hinder the electron transfer. The introduction of complementary hydroxymethylated DNA (containing 5hmC) further hinders the electron transfer (curve e), due to the negatively charged phosphate backbone of the oligonucleotides repelling the redox probe from the electrode surface. The R_{et} value increases again when the electrode was incubated with β-GT (curve f), due to the insulating effect and negative charge of glucose. Finally, capture of the B-CDs by the transferred glucose groups reduces the R_{et} value (curve g), which is rationalized by the increased area of the electrode and acceleration of the electron transfer. The EIS data in Fig. 2A thus confirms that each stage of the biosensor fabrication process is successful.

In order to verify the feasibility of the biosensor, the photocurrent response of the various modified electrodes in 0.1 M PBS containing 0.1 M AA (pH = 7.4) were measured and compared. Fig. 2B shows that a strong response is obtained for the WS_2/ITO electrode (curve a), indicating that WS_2 nanosheets possess good photoactivity. The photocurrent increases after introducing AuNPs (curve b), indicating that the AuNPs facilitate electron separation and transfer in WS_2 whilst also increasing the electrode surface area. It should be noted that the AuNPs also absorb visible light via their localized surface plasmon resonance

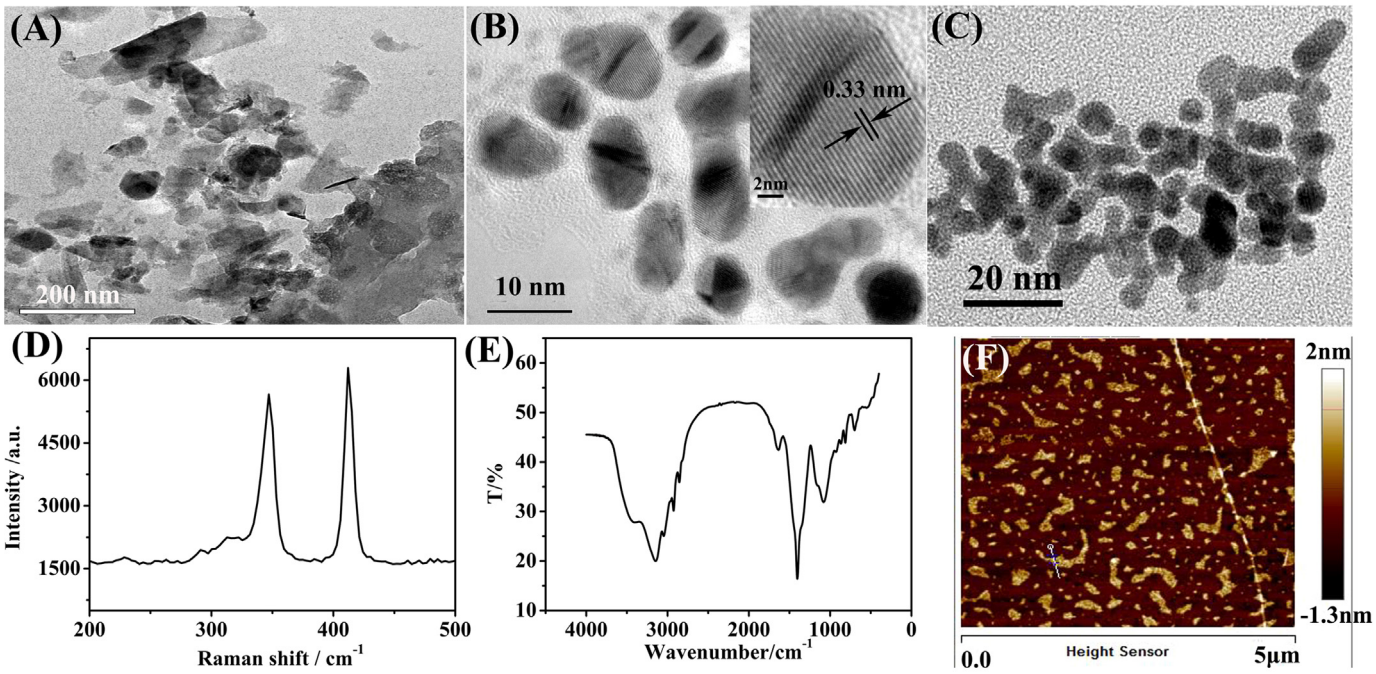

Fig. 1. (A) TEM image of WS_2 nanosheets, (B) HRTEM images of B-CDs (C) TEM image of AuNPs, (D) Raman spectrum of WS_2 nanosheets, (E) FT-IR spectrum of B-CDs, (F) AFM images of the WS_2 nanosheets.

(LSPR), and thus plasmonic effects may have been contributed to the increased photocurrent. The photocurrent decreases when the probe DNA and complementary hydroxymethylated DNA were immobilized on electrode surface (curve c). This is explained by the insulating and spatial effects of DNA, which may have partially blocked light reaching the WS_2 layer, thereby reducing the number of charge carriers created under light irradiation. In agreement with this hypothesis, the photocurrent decreases further after incubating the electrode with β-GT (curve d). Finally, the photocurrent increases considerably after the B-CDs were captured on the electrode (curve e). This is attributed to excellent electron transfer properties and the energy-down-shift effect of the CDs.

The capture of B-CDs is thus crucial to the PEC performance of the biosensor. The capture involves glucose groups, which are introduced by the reaction of immobilized hydroxymethylated DNA with β-GT. To confirm the key role of the glucose groups in B-CDs capture, two control experiments were performed. Firstly, ssDNA/AuNPs/WS_2/ITO was incubated with β-GT and B-CDs, and the PEC performance of the resulting electrode recorded in detection buffer. As shown in Fig. 2B. (curve f), the measured photocurrent is much lower than that measured for B-CDs/Glu/5hmC-dsDNA/AuNPs/WS_2/ITO. The result establishes that B-CDs are not fixed on the electrode surface in the absence of hydroxymethylated DNA. Next, when 5hmC-dsDNA/AuNPs/WS_2/ITO was incubated with only B-CDs (no β-GT), the photocurrent (curve g) is almost identical to that determined for the 5hmC-dsDNA/AuNPs/WS_2/ITO electrode. This suggests that B-CDs do not assemble directly on the electrode surface without the glucose groups. These control experiments conclusively demonstrate the sensitive detection of hydroxymethylated DNA and an activity assay for β-GT could be achieved using the developed biosensor.

3.3. Performance of the biosensor for hydroxymethylated DNA detection

Under the optimized experimental conditions (see Supplementary Materials), the potential of the PEC biosensor to detect hydroxymethylated DNA was explored. Fig. 3A shows that the photocurrent increases with increasing hydroxymethylated DNA concentration from 0.01 to 100 nM. The photocurrent shows a linear dependence on the logarithm of the hydroxymethylated DNA concentration (Fig. 3B), as described by the equation of I (nA) = 341.07 log$c$ (nM) + 1111.13 (R = 0.9937, the linear regression coefficient is 0.9874, and the error bars in each plot represent the standard deviation of three measurements). The detection limit was calculated to be 0.0034 nM (S/N = 3). Compared with previous strategies for detection of hydroxymethylated DNA

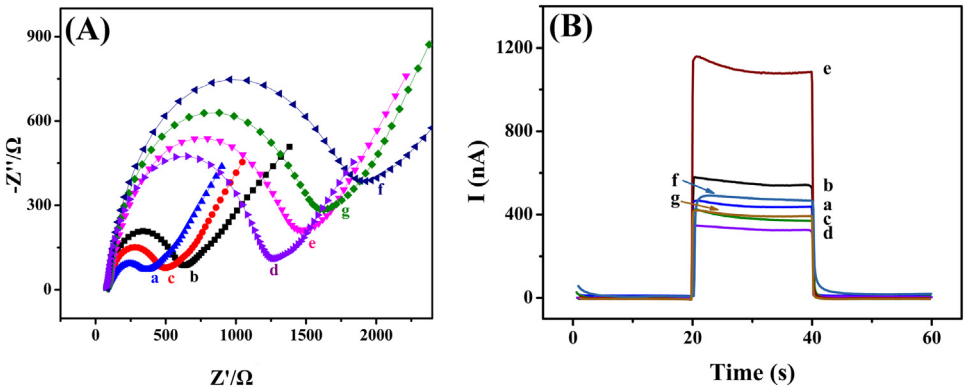

Fig. 2. (A) EIS of ITO (a), WS_2/ITO (b), AuNPs/WS_2/ITO (c), ssDNA/AuNPs/WS_2/ITO (d), 5hmC-dsDNA/AuNPs/WS_2/ITO (e), Glu/5hmC-dsDNA/AuNPs/WS_2/ITO (f), CQDs/Glu/5hmC-dsDNA/AuNPs/WS_2/ITO (g) in 5 mM $K_3[Fe(CN)_6]/K_4[Fe(CN)_6]$ (1:1) containing 0.1 M KCl. (B) PEC response of WS_2/ITO (a), AuNPs/WS_2/ITO (b), 5hmC-dsDNA/AuNPs/WS_2/ITO (c), Glu/5hmC-dsDNA/AuNPs/WS_2/ITO (d), B-CDs/Glu/5hmC-dsDNA/AuNPs/WS_2/ITO (e), ssDNA/AuNPs/WS_2/ITO after incubation with β-GT and B-CDs (f), 5hmC-dsDNA/AuNPs/WS_2/ITO after incubation with B-CDs (g). All data was collected in 0.1 M PBS containing 0.1 M AA (pH = 7.4).

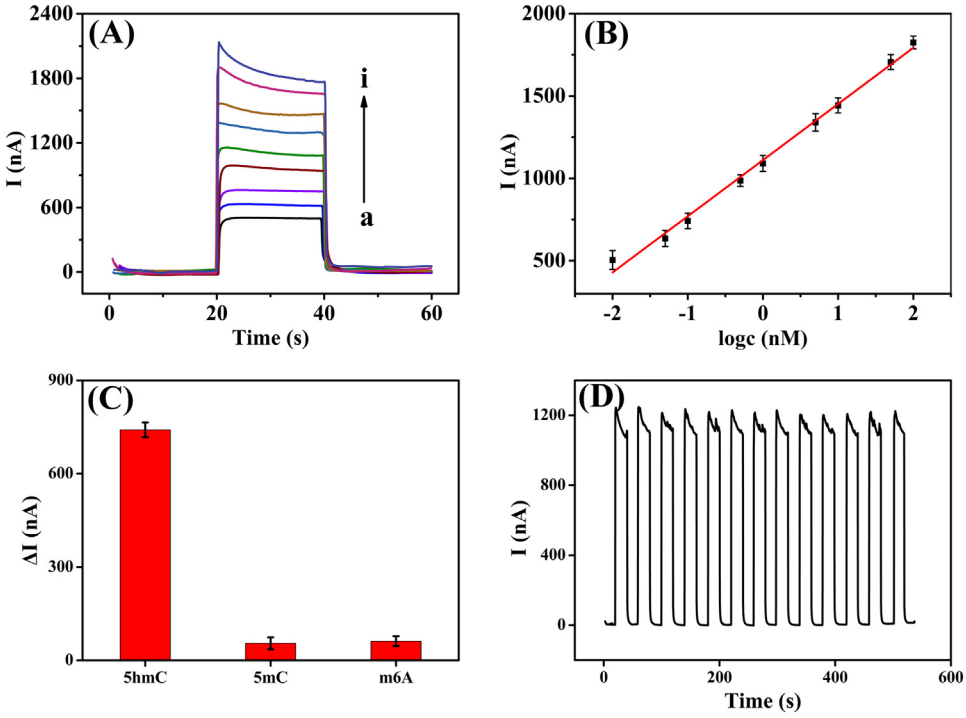

Fig. 3. (A) Photocurrent responses of the PEC biosensor to different concentrations of hydroxymethylated DNA. a-i, 0.01, 0.05, 0.1, 0.5, 1, 5, 10, 50, 100 nM (the concentration of β-GT was 60 unit/mL). (B) Calibration curve of PEC response versus hydroxymethylated DNA concentration. (C) Selectivity of the biosensor. (D) Time–based photocurrent response of the biosensor in 0.1 M PBS containing 0.1 M AA (pH 7.4) with light on and off cycles.

Table 1
Performance comparison of the photoelectrochemical biosensor with other methods developed for hydroxymethylated DNA detection.

Methods	Linear range (nM)	LOD (nM)	Reference
Capillary electrophoresis	0.09–90	0.09	(Krais et al., 2011)
Electrochemiluminescence	0.05–10	0.0163	(Zhang et al., 2017)
Electrochemiluminescence	0.0005–0.1	0.00014	(Ma et al., 2016)
Electrochemiluminescence	0.1–30	0.047	(Jiang et al., 2018a)
Fluorescence	0–100	0.167	(Chen et al., 2017)
Fluorescence	0.1–2	–	(Hu et al., 2014)
Electrochemistry	0.5–90	0.14	(Yin et al., 2017)
Electrochemistry	0.1–30	0.032	(Yang et al., 2015)
PEC	0.01–100	0.0034	This work

(see Table 1), this PEC biosensor exhibits a lower detection limit and a wider linear range.

Excellent selectivity, stability and reproducibility are essential condition for a practical biosensor. To investigate the selectivity of the PEC biosensor, methylated DNA and methylated RNA were selected as potential interferants. Modified electrodes were constructed using methylated DNA or methylated RNA, and the photocurrent change ($\Delta I = I_2 - I_1$) was compared, where I_1 represents the photocurrent of the ssDNA/AuNPs/WS_2/ITO electrode coated with 1 nM of 5hmC-DNA, methylated DNA or methylated RNA, and I_2 represents the photocurrent of the biosensor (fabricated with 1 nM of 5hmC-dsDNA, methylated DNA or methylated RNA). As can been seen from Fig. 3C, the photocurrent changes of the biosensor to hydroxymethylated DNA is much higher than that to other potential interferents, indicating that the PEC biosensor shows a remarkable selectivity for hydroxymethylated DNA.

The stability of the PEC biosensor was also explored. The photocurrent of the B-CDs/Glu/5hmC-dsDNA/AuNPs/WS_2/ITO biosensor was evaluated in detection buffer over a number of light on and off cycles (13 cycles over 540 s, Fig. 3D). No significant change in the photocurrent response is observed during the cycle tests, with the relative standard deviation (RSD) of the PEC response being only 1.06%, indicating that this PEC biosensor demonstrated excellent stability. The reproducibility of the PEC biosensor was investigated by comparing the photocurrent of seven B-CDs/Glu/5hmC-dsDNA/AuNPs/WS_2/ITO electrodes fabricated at the same time. No significant differences are found in the photocurrent of these seven independent PEC biosensors (RSD 1.54%), indicating that the biosensor has good reproducibility.

3.4. Analysis of β-GT activity

Under the optimized experimental conditions (see Supplementary materials), the performances of the PEC biosensor to detect β-GT activity were explored. As shown in Fig. 4A, the photocurrent increases with increasing β-GT concentration in the range of 0.1–220 unit/mL. A linear relationship is found between the photocurrent and the logarithm of β-GT concentration in the range from 0.1 u to 220 unit/mL (inset of Fig. 4A). The linear regression equation is I (nA) = 205.30 log$c$ (unit/mL) + 716.03, (R = 0.9975, the linear regression coefficient is 0.9950, and the error bars in each plot represent the standard deviation of three measurements). The detection limit of β-GT was approximately 0.028 unit/mL (S/N = 3). Compared with previous strategies for detection of β-GT activity (Jiang et al., 2018b; Sun et al., 2016; Yin et al., 2017) (see Table S1), the PEC biosensor exhibits a lower detection limit and a wider linear range.

The selectivity of the biosensor for β-GT activity was also examined using β-GAT and UGT2B7 as the model interfering agents. For comparison purposes, we used the change of photocurrent ($\Delta I = I_2 - I_1$), where I_1 represents the photocurrent of the 5hmC-dsDNA/AuNPs/WS_2/ITO electrode and I_2 represents the photocurrent of the biosensor (fabricated with 60 unit/mL of β-GT, β-GAT or UGT2B7). As can been seen from Fig. 4B, the photocurrent change of the biosensor to β-GT is much higher than that of other potential interferents, indicating the remarkable selectivity for β-GT detection of this PEC biosensor.

β-GT transfers a glucose group from UDP-Glu to 5hmC residue in DNA. Therefore, it is of interest to see if the biosensor could be used to screen inhibitors of β-GT. The inhibitor screening assay was performed using 4-phenylimidazole as a model inhibitor. As shown in Fig. 4C, the photocurrent of the biosensor decreases with increasing inhibitor concentration in the range of 0–40 μM, indicating that the inhibition of β-GT by 4-phenylimidazole is dose-dependent. The inhibition ration

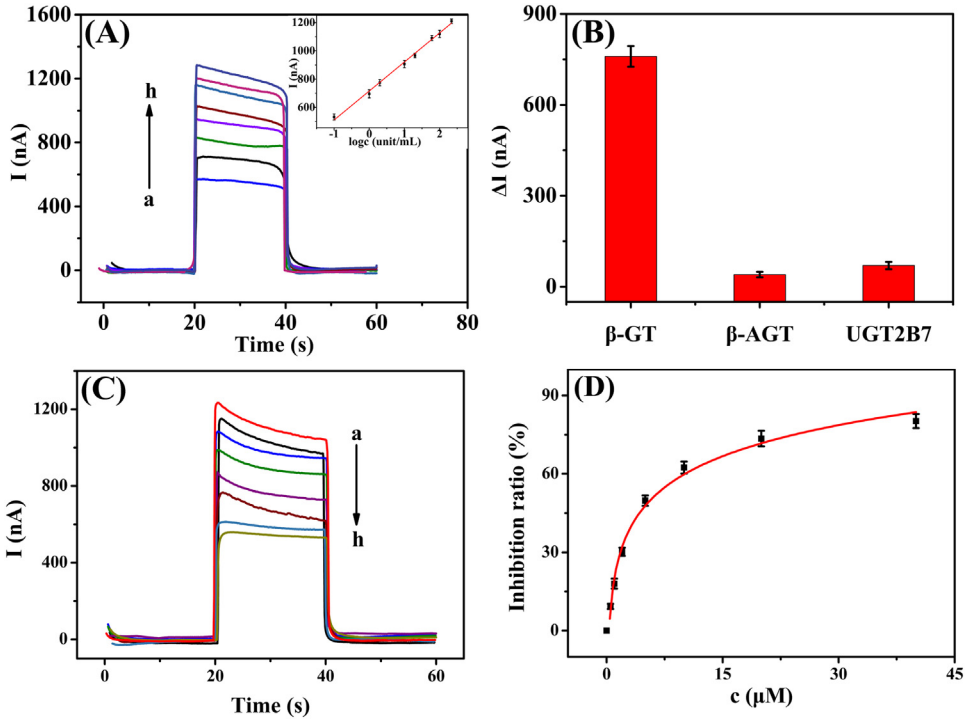

Fig. 4. (A) Photocurrent responses of the PEC biosensor to different concentrations of β-GT. a-h, 0.1, 1, 5, 10, 20, 60, 100, 220 unit/mL (the concentration of hydroxymethylated DNA was 1 nM). Inset: calibration curve of PEC response versus β-GT concentration. (B) Selectivity for the detection of β-GT. (C) PEC response of the biosensor in the presence of different concentrations of 4-phenylimidazole. a-h, 0, 0.5, 1, 2, 5, 10, 20 and 40 μM. The β-GT concentration was 60 unit/mL. (D) Plot of the inhibition percent versus 4-phenylimidazole concentration.

shows a logarithm dependence on the 4-phenylimidazole concentration (Fig. 4D), as described by the inhibition ration (%) = a – bln(c (nM) + d) (a = 20.578 ± 4.2013, b = -17.053 ± 1.5381, d = -0.020 ± 0.1926). The IC_{50} (half maximal inhibitory concentration) was calculated to be 5.06 μM (Fig. 4D), which is comparable with some previous results, such as 2.14 μM (Yin et al., 2017), 4.22 μM (Jiang et al., 2018b), 4.75 μM (Sun et al., 2016). The result confirms that the biosensor displays promise for the screening of β-GT inhibitors.

4. Conclusions

In summary, a simple and low-cost PEC biosensor was successfully developed for the sensitive detection of 5-hydroxymethylcytosine, and β-GT activity measurement (including inhibitor screening). Under optimized testing conditions, the biosensor showed a wide linear response with 5hmC and β-GT concentration from 0.01 to 100 nM and 0.1–220 unit/mL, low detection limits which were 0.0034 nM and 0.028 unit/mL respectively, excellent selectivity, stability and reproducibility. Moreover, the proposed method could be easily extended to screen β-GT inhibitors, which might be helpful for the discovery of anticancer drugs. However, this work also has some shortcomings, such as that, it cannot achieve the detection of 5hmC in genome and vivo. Future work may include further optimizing of the biosensor, developing integrated sensing system, and expanding its applications to monitor 5hmC in vivo.

Acknowledgments

This work was supported by the National Natural Science Foundation of China (Nos. 21775090, 41807484, 21675140 and 21375079), the Natural Science Foundation of Shandong Province, China (Nos. ZR2016BM10 and ZR2018MB028). GINW acknowledges funding support from the Dodd Walls Centre for Photonic and Quantum Technologies. Dr Qin Xu acknowledges funding support from the 14th Six Talent Peaks Project in Jiangsu Province (SWYY-085), Young Academic Leaders of Jiangsu Province (2018), the project funded by the PAPD and TAP.

Declaration of interest statement

There are no conflicts of interest.

Appendix A. Supplementary material

Supplementary data associated with this article can be found in the online version at doi:10.1016/j.bios.2018.11.054.

References

Chen, H.-y., Wei, J.-R., Pan, J.-X., Zhang, W., Dang, F.-q., Zhang, Z.-Q., Zhang, J., 2017. Biosens. Bioelectron. 91, 328–333.
Chen, S., Dou, Y., Zhao, Z., Li, F., Su, J., Fan, C., Song, S., 2016. Anal. Chem. 88 (7), 3476–3480.
Flusberg, B.A., Webster, D.R., Lee, J.H., Travers, K.J., Olivares, E.C., Clark, T.A., Korlach, J., Turner, S.W., 2010. Nat. Methods 7, 461.
Ge, J., Xin, G., Du, Y.-H., Chen, J.-J., Zhang, L., Bai, D.-M., Ji, D.-Y., Hu, Y.-L., Li, Z.-H., 2017. Sens. Actuat. B: Chem. 249, 189–194.
Ge, L., Wang, W., Hou, T., Li, F., 2016. Biosens. Bioelectron. 77, 220–226.
Guo, J., 2016. Anal. Chem. 88 (24), 11986–11989.
Guo, J., 2017. Anal. Chem. 89 (17), 8609–8613.
Guo, J., Huang, X., Ma, X., 2018. Sens. Actuat. B: Chem. 275, 446–450.
Guo, J., Ma, X., 2017. Biosens. Bioelectron. 94, 415–419.
Hou, T., Xu, N., Wang, W., Ge, L., Li, F., 2018. Anal. Chem. 90 (15), 9591–9597.
Hou, T., Zhang, L., Sun, X., Li, F., 2016. Biosens. Bioelectron. 75, 359–364.
Hu, J., Chen, Y., Xu, X., Wu, F., Xing, X., Xu, Z., Xu, J., Weng, X., Zhou, X., 2014. Bioorg. Med. Chem. Lett. 24 (1), 294–297.
Ito, S., D'Alessio, A.C., Taranova, O.V., Hong, K., Sowers, L.C., Zhang, Y., 2010. Nature 466, 1129.
Jiang, W., Wu, L., Duan, J., Yin, H., Ai, S., 2018a. Biosens. Bioelectron. 99, 660–666.
Jiang, W., Yin, H., Zhou, Y., Duan, J., Li, H., Wang, M., Waterhouse, G.I.N., Ai, S., 2018b. Sens. Actuat. B: Chem. 274, 144–151.
Krais, A.M., Park, Y.J., Plass, C., Schmeiser, H.H., 2011. Epigenetics 6 (5), 560–565.
Kriaucionis, S., Heintz, N., 2009. Science 324 (5929), 929–930.
Li, X., Zhu, L., Zhou, Y., Yin, H., Ai, S., 2017a. Anal. Chem. 89 (4), 2369–2376.
Li, Y., Tian, J., Yuan, T., Wang, P., Lu, J., 2017b. Sens. Actuat. B: Chem. 240, 785–792.
Münzel, M., Globisch, D., Carell, T., 2011. Angew. Chem. Int. Ed. 50 (29), 6460–6468.
Ma, S., Sun, H., Li, Y., Qi, H., Zheng, J., 2016. Anal. Chem. 88 (20), 9934–9940.
Mo, L., Li, J., Liu, Q., Qiu, L., Tan, W., 2017. Biosens. Bioelectron. 89, 201–211.
Okoth, O.K., Yan, K., Liu, Y., Zhang, J., 2016. Biosens. Bioelectron. 86, 636–642.
Sukovich, D.J., Modavi, C., de Raad, M., Prince, R.N., Anderson, J.C., 2015. ACS Synth. Biol. 4 (7), 833–841.
Sun, H., Ma, S., Li, Y., Qi, H., Ning, X., Zheng, J., 2016. Biosens. Bioelectron. 79, 92–97.
Tan, Y., Li, M., Ye, X., Wang, Z., Wang, Y., Li, C., 2018. Sens. Actuat. B: Chem. 262, 982–990.

Xie, H., Dong, J., Duan, J., Waterhouse, G.I.N., Hou, J., Ai, S., 2018. Sens. Actuat. B: Chem. 259, 1082–1089.
Xu, Z.-Q., Zhang, Y., Lin, S., Zheng, C., Zhong, Y.L., Xia, X., Li, Z., Sophia, P.J., Fuhrer, M.S., Cheng, Y.-B., Bao, Q., 2015. ACS Nano 9 (6), 6178–6187.
Yan, K., Liu, Y., Yang, Y., Zhang, J., 2015. Anal. Chem. 87 (24), 12215–12220.
Yang, Z., Jiang, W., Liu, F., Zhou, Y., Yin, H., Ai, S., 2015. Chem. Commun. 51 (78), 14671–14673.
Yin, H., Yang, Z., Wang, H., Zhou, Y., Ai, S., 2017. Sens. Actuat. B: Chem. 243, 602–608.
Yin, R., Mo, J., Lu, M., Wang, H., 2015. Anal. Chem. 87 (3), 1846–1852.
Zang, Y., Lei, J., Hao, Q., Ju, H., 2016. Biosens. Bioelectron. 77, 557–564.
Zhang, Y., Li, Y., Wei, Y., Sun, H., Wang, H., 2017. Talanta 170, 546–551.
Zhao, W.-W., Xu, J.-J., Chen, H.-Y., 2014. Chem. Rev. 114 (15), 7421–7441.